(Received 30 July 2023, Accepted 15 November 2023, Scheduled 2 February 2024)

# Fault-Tolerant Control of D-PMSG Demagnetization Based on Linear Active Disturbance Rejection Controller

Bing Luo[1], Bozhong Liu[1], Sicheng Peng[2], Zhi Yu[1], and Yang Zhang[1,*]

[1]*Hunan University of Technology, Zhuzhou 412007, China*
[2]*State Grid Hunan Extra High Voltage Transmission Company, Changsha 410000, China*

**ABSTRACT:** When demagnetization occurs, direct-drive permanent magnet synchronous wind generator exhibits problems of poor dynamic performance, weak immunity to disturbances and speed fluctuations. Aiming at these problems, this paper proposes a cascaded linear active disturbance rejection control method. First, the mathematical models of the generator during normal operation and demagnetization are described. Second, the linear active disturbance rejection controller (LADRC) for the speed and current loops is designed. The compensation for demagnetization disturbances at the speed loop's input is enabled by the control approach. The current output of the speed loop is imported as a rated value into the LADRC of the current loop. At the same time, the current is compensated at the input. Compensated speed and current accurately track the given values, and the goal of achieving demagnetization fault tolerance is met. Finally, this method is compared with dual-loop Proportional Integral (PI) control. The experimental results affirm that, under this control method, when demagnetization occurs, the speed fluctuation is reduced by 95.7%, the current response time decreased from 0.01 seconds to 0.001 seconds, and the electromagnetic torque ripple amplitude reduced by 50%. These experimental results fully validate the heightened fault tolerance and resistance to interference exhibited by the method advocated in this paper.

## 1. INTRODUCTION

Direct-drive permanent magnet synchronous generator (D-PMSG) is the hot spot of wind power development nowadays [1–3]. In harsh environments, D-PMSG systems may be susceptible to demagnetization failures caused by elevated temperatures, chemical corrosion, mechanical vibrations, and other factors [4–6]. During the demagnetization of permanent magnets, magnetic induction continuously decreases. When the demagnetization characteristics of the worst operating point during transient processes [7] are considered, a sudden decrease in magnetic induction at constant system prime mover causes a decrease in electromagnetic torque. The stator current increases to compensate for the missing torque, while speed fluctuations occur. The generator will correspond to an optimal speed for each wind speed. A mismatch between actual and rated speeds may lead to the generator operating below its maximum performance efficiency point [8, 9]. Therefore, it is essential to maintain the rotation speed stability during demagnetization.

Nowadays, a prevalent approach in wind power generation involves a dual-loop Proportional Integral (PI) control for the generator system [10, 11]. PI controllers have the advantages of easy debugging and fast response time, but they also have three drawbacks [12, 13]. First, the PI controller is based on error feedback to eliminate errors. This approach can lead to significant system overshooting due to an excessive initial control force, resulting in an imbalanced trade-off between speed and overshoot. The second problem is that disturbances are frequent in wind turbine control. PI gain needs to be adjusted to the environment, so complex PI controller parameterization schemes are required. Third, the integration link inside the PI regulator can make the system dynamic performance worse and affect the current compensation speed. Therefore, when demagnetization occurs, PI controllers are often unable to quickly eliminate speed fluctuations.

Some scholars have proposed new control methods to enhance the system's immunity to interference. Ref. [14] introduced a model-based high-order sliding mode controller, which can ensure tracking of generator reference speed while increasing system performance. However, sliding mode controllers have oscillation problem. Ref. [15] proposed a dual-vector model predictive fault-tolerant controller, which suppresses the speed change of the D-PMSG during demagnetization by controlling the stator current. However, the paper mainly considers the case of insufficient stator current compensation during demagnetization. Speed fluctuations persisted during demagnetization despite this method. Ref. [16] used an integrated controller based on a model predictive controller and an expanded state observer, eliminating speed overshoot through controller inertia recognition technology. However, the current loop still uses a PI controller, resulting in insufficient dynamic response of the current. In addition, most of the currently known fault-tolerant control methods for generators require advance knowledge of a comprehensive mathematical system characterization. Acquiring an accurate mathematical model of the physical system is frequently complex. Therefore, it is particularly impor-

* Corresponding authors: Yang Zhang (459387623@qq.com).

tant to study a controller with a simple structure that is independent of the mathematical system model.

The active disturbance rejection control (ADRC) method is an active anti-interference strategy pioneered by Han [17]. Under this control method, all uncertain elements impacting the target to be controlled are summarized as "unknown disturbances". The output and input data of the object to be controlled are used for compensation. This control method has the characteristics of not relying on the model of the control object and not distinguishing between external and internal perturbations. Gao [18] proposed a linear active disturbance rejection control method for the difficult problem of traditional ADRC parameter tuning. Some scholars have utilized the ADRC technique in motor control, which has resulted in a significant improvement in the performance of the motor. Ref. [19] proposed a vector control approach for permanent magnet synchronous motor based on ADRC controller, which consists of both a current controller and an ADRC speed loop. This method has better dynamic tracking performance than conventional control strategy. Ref. [20] introduced an innovative approach, incorporating rapid space vector pulse width modulation (SVPWM) and switching structures, which are founded on sliding mode control (SMC) and active disturbance rejection control. This method improves the pulse modulation and harmonic suppression of the system. Ref. [21] introduced ADRC into the speed ring of permanent magnet synchronous wind power generation system. Compared with the traditional PI regulator, the dynamic build-up of the DC bus voltage is closer to the target required for steady state operation control. Ref. [22] presented an LADRC-based current controller, which simplifies the parameter tuning process and eliminates current oscillations.

In summary, there have been some researches based on the ADRC technique. The results show that the ADRC technique can be used in PMSM to enhance the robustness of the motors. The use in generators can enhance the harmonic suppression and improve the steady state operation characteristic. However, there are fewer studies on the anti-interference capability of ADRC technology in D-PMSG, especially for the generator fault-tolerant control when demagnetization faults occur.

Aiming at the problem of poor dynamic performance, weak immunity, and speed fluctuations when direct-drive permanent magnet synchronous wind generator is subjected to demagnetization perturbation, this paper proposes a cascaded LADRC control method. The mathematical model of D-PMSG during normal and demagnetization is described, and then the LADRC of the speed and current loops are designed. The demagnetization disturbances are compensated at the inputs to enable the speed and current tracking the given values accurately, thus achieving the fault-tolerant control. The control method introduced in this paper demonstrates exceptional performance in substantially mitigating speed fluctuations during demagnetization. Additionally, reductions have been achieved in current response time, harmonic distortion rate, and electromagnetic torque ripple amplitude. Experimental validation has conclusively demonstrated the robust fault tolerance and anti-interference capabilities inherent in the control approach proposed in this paper.

## 2. D-PMSG MATHEMATICAL DESCRIPTION

### 2.1. Mathematical Model of D-PMSG During Normal Operation

D-PMSG generally uses surface-mounted permanent magnet synchronous generators. The PMSG mathematical model in synchronous rotation of a coordinate system based on rotor magnetic chain orientation can be stated as follows:

$$\begin{cases} u_d = R_s i_d + L_d \dfrac{di_d}{dt} - \omega_e L_q i_q \\ u_q = R_s i_q + L_q \dfrac{di_q}{dt} + \omega_e L_d i_d + \omega_e \psi_{r0} \end{cases} \tag{1}$$

where $u_d$ and $u_q$, respectively, represent the $d$- and $q$-axis stator voltages; $i_d$ and $i_q$ are the $d$- and $q$-axis currents, respectively; $L_d$ and $L_q$ are $d$- and $q$-axis stator inductances, respectively; $R$ is the stator resistance; $\psi_{r0}$ is the flux linkage of the rotor permanent magnet; $\omega_e$ is the electrical rotor speed.

The flux-linkage equation is expressed as follows:

$$\begin{cases} \psi_d = L_d i_d + \psi_{r0} \\ \psi_q = L_q i_q \end{cases} \tag{2}$$

where $\psi_d$ and $\psi_q$ represent the flux linkages in the $d$-axis and $q$-axis, respectively.

The speed equation and electromagnetic torque equation of the D-PMSG can be stated as follows:

$$\begin{cases} Jp\omega_m = T_L - T_e - B\omega_m \\ T_e = 1.5 n_p \left[\psi_{r0} + (L_d - L_q) i_d\right] i_q \end{cases} \tag{3}$$

where $J$ represents the Inertia moment; $\omega_m$ is mechanical rotor speed; $T_e$ is the electromagnetic torque; $T_L$ is the mechanical torque; $n_p$ is polar logarithms.

### 2.2. Mathematical Modeling of the Occurrence of Demagnetization Faults

When motor permanent magnets face demagnetization failure, both the direction and amplitude of the PM flux linkage will change. The amplitude of the flux linkage shifts from its initial value $\psi_{ro}$ to $\psi_r$, with an angle difference between the flux vector direction of the rotor and the reference frame's $d$-component, as depicted in Figure 1.

As depicted in Figure 1, the permanent magnet flux relationship equation in the D-PMSG under demagnetization fault can be stated as:

$$\begin{cases} \psi_{rd} = \cos\gamma \psi_r \\ \psi_{rq} = \sin\gamma \psi_r \end{cases} \tag{4}$$

where $\psi_{rd}$ and $\psi_{rq}$ represent the flux linkages in the $d$-axis and $q$-axis of the permanent magnet, respectively.

The equation for the stator flux linkage of a D-PMSG during demagnetization fault can be stated as:

$$\begin{cases} \psi_d = \psi_{rd} + L_d i_d \\ \psi_q = \psi_{rq} + L_q i_q \end{cases} \tag{5}$$

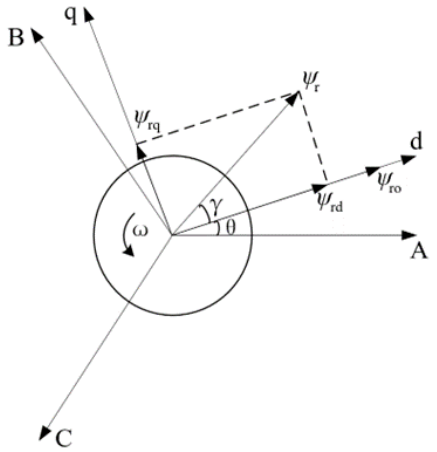


**FIGURE 1**. Change in the flux linkage of the D-PMSG.

where $\psi_d$ and $\psi_q$ represent the stator flux linkages in the $d$-axis and $q$-axis, respectively.

Expressions describing the speed and electromagnetic torque in the D-PMSG under demagnetization can be stated as:

$$\begin{cases} J\dfrac{d\omega_m}{dt} = T_L - T_e - B\omega_m \\ T_e = 1.5n_p\left[(\psi_{rd} + L_d i_d - L_q i_d)i_q - \psi_{rq} i_d\right] \end{cases} \tag{6}$$

When a demagnetization fault occurs in the permanent magnet generator, the state equations of the D-PMSG in the $d$-axis and $q$-axis reference frames can be stated as:

$$\begin{cases} \dfrac{di_d}{dt} = -\dfrac{R_S}{L_d} i_d + \omega_e \dfrac{L_q}{L_d} i_q + \dfrac{u_d}{L_d} + \omega_e \dfrac{\psi_{rq}}{L_d} \\ \dfrac{di_q}{dt} = -\dfrac{R_S}{L_q} i_q - \omega_e \dfrac{L_d}{L_q} i_d + \dfrac{u_q}{L_q} - \omega_e \dfrac{\psi_{rd}}{L_q} \end{cases} \tag{7}$$

For surface D-PMSG, $L_d = L_q$.

## 3. VECTOR CONTROL BASED ON CASCADED LINEAR ACTIVE DISTURBANCE REJECTION CONTROL

LADRC has the characteristics of simple structure, easy performance analysis, and parameter tuning, so this control method is more suitable to be applied in D-PMSG. The core components of LADRC are the linear extended state observer (LESO) and linear state error feedback (LSEF) control rate. The concrete design methodology is described in the following section.

### 3.1. Speed Loop LADRC Controller Design

In order to solve the overshooting problem during the speed rise process and to obtain better steady state characteristics, a linear tracking differentiator (LTD) is designed for prearranging the transition process. The formula for LTD is expressed as follows:

$$\begin{cases} e_1 = v_1 - \omega_m^* \\ pv_1 = -re_1 \end{cases} \tag{8}$$

where $\omega_m^*$ represents the reference rotational speed value supplied to the LTD module; $v_1$ is the value of the rotational speed output from the LTD link; $e_1$ is the difference between the speed input and output; $r$ represents the speed factor; $p$ represents the differential operator.

LESO can estimate the real-time contribution of perturbations inside and outside the system, with the perturbations due to demagnetization included in the design of equation. From Eq. (6), the speed equation of state can be stated as:

$$p\omega_m = f_\omega + b_\omega i_q \tag{9}$$

where $\omega_m$ and $i_q$ are used here as the output and input quantities of the speed loop LADRC, respectively; $f_\omega$ is the total disturbance of the speed ring, $f_\omega = 1/J(T_L - 1.5n_p i_q \psi_{rd} - \beta\omega_m) - b_\omega i_q$; $b_\omega$ is the current scaling factor.

Selecting state variables as $x_1 = \omega_m, x_2 = f_\omega$, the extended equation of state is then expressed as:

$$\begin{cases} px_1 = x_2 + b_\omega i_q \\ px_2 = pf_\omega \\ y_1 = x_1 \end{cases} \tag{10}$$

where $y_1$ is the output of the LESO link.

Based on this extended state equation, a LESO such as Eq. (11) can be designed:

$$\begin{cases} e_2 = z_1 - \omega_m \\ pz_1 = z_2 - \beta_1 e_2 + b_\omega i_q \\ pz_2 = -\beta_2 e_2 \end{cases} \tag{11}$$

where $e_2$ is the error between the estimated value of speed and the actual value of speed; $z_1$ is employed for estimating the state of $\omega_m$; $z_2$ is employed for estimating the real time value of the total perturbation $f_\omega$; $\beta_1$ and $\beta_2$ represent the gains for correcting output errors.

LSEF can control and compensate for disturbances using the signals derived from the LTD and the system output observed by the LESO. Simple first-order LADRC allows for the application of proportional control, which can be expressed in terms of the equation as:

$$u_{01} = k_{p1}(v_1 - z_1) \tag{12}$$

where $u_{01}$ is the equivalent control quantity; $k_{p1}$ is the control parameter.

Finally, the estimated perturbations are compensated in the control input to obtain the output equation:

$$u_1 = \frac{1}{b_\omega}(u_{01} - z_2) \tag{13}$$

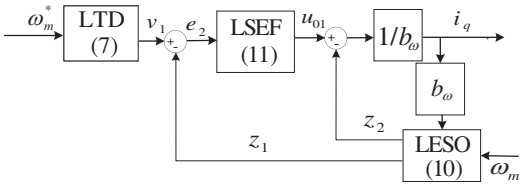


**FIGURE 2**. D-PMSG speed ring LADRC controller.

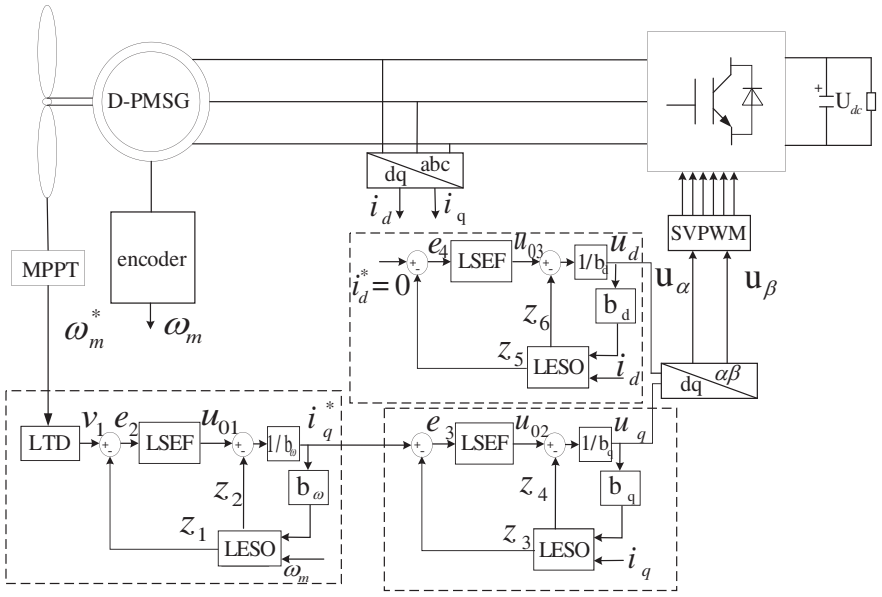


**FIGURE 3**. Block diagram of D-PMSG fault-tolerant control system based on cascaded LADRC.

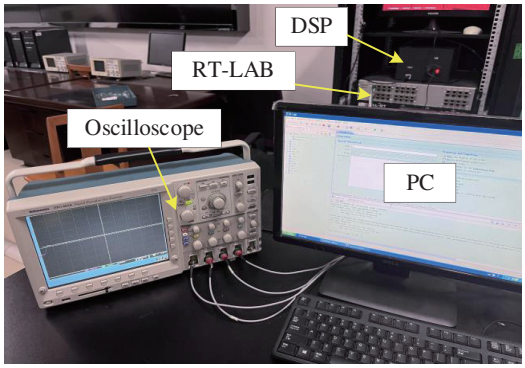


**FIGURE 4**. Rt-lab platform.

where $u_1$ is the output of the LSEF.

Figure 2 depicts the structural block diagram.

### 3.2. Current Loop Ladrc Controller Design

After the generator is demagnetized, the stator current increases to compensate for the missing electromagnetic torque, and the dynamic feed-forward from the LESO and LSEF of the LADRC controller provides higher tracking accuracy and thus improves the current response.

Using the $q$-axis current loop as an illustration to design the LADRC, from Eq. (7), the current equation of state can be expressed as:

$$pi_q = \frac{1}{L_q}[u_q - R_s i_q - \omega_e(L_d i_d + \psi_{rd})] \tag{14}$$

Let $f_q$ be the total disturbances that contain the changes in the magnetic chain, $f_q = 1/L_q\,[u_q - Ri_q - \omega_e(L_d i_d + \psi_{rd})] - b_q u_q$. The state equation for current can be stated as:

$$pi_q = f_q + b_q u_q \tag{15}$$

As the current loop demands a rapid response, we do not introduce a transition process for the predefined current value. Instead, the reference current for the $q$-axis is generated through the speed loop controller. We have chosen state variables $x_3 = i_q$ and $x_4 = f_q$. The extended state equation for the current loop is as follows:

$$\begin{cases} px_4 = x_4 + b_q u_q \\ px_4 = pf_q \\ y_2 = x_3 \end{cases} \tag{16}$$

where $y_2$ is the output of the LESO link.

Figure 3 shows the overall block diagram of D-PMSG fault-tolerant control system based on cascaded LADRC proposed in the paper. Referring to the rotational speed ring LADRC design scheme, the $q$-axis current ring LADRC discretization equation can be summarized as follows, and the $d$-axis current LADRC discretization equation is obtained by the same reason:

$$\begin{cases} e_3 = z_3 - i_q \\ pz_3 = z_4 - \beta_3 e_3 + b_q u_q \\ pz_4 = -\beta_4 e_3 \\ u_{02} = k_{p2}(i_q^* - z_3) \\ u_2 = \dfrac{1}{b_q}(u_{02} - z_4) \end{cases} \tag{17}$$

$$\begin{cases} e_4 = z_5 - i_d \\ pz_5 = z_6 - \beta_5 e_4 + b_d u_d \\ pz_6 = -\beta_6 e_4 \\ u_{03} = k_{p3}(i_d^* - z_5) \\ u_3 = \dfrac{1}{b_d}(u_{03} - z_6) \end{cases} \tag{18}$$

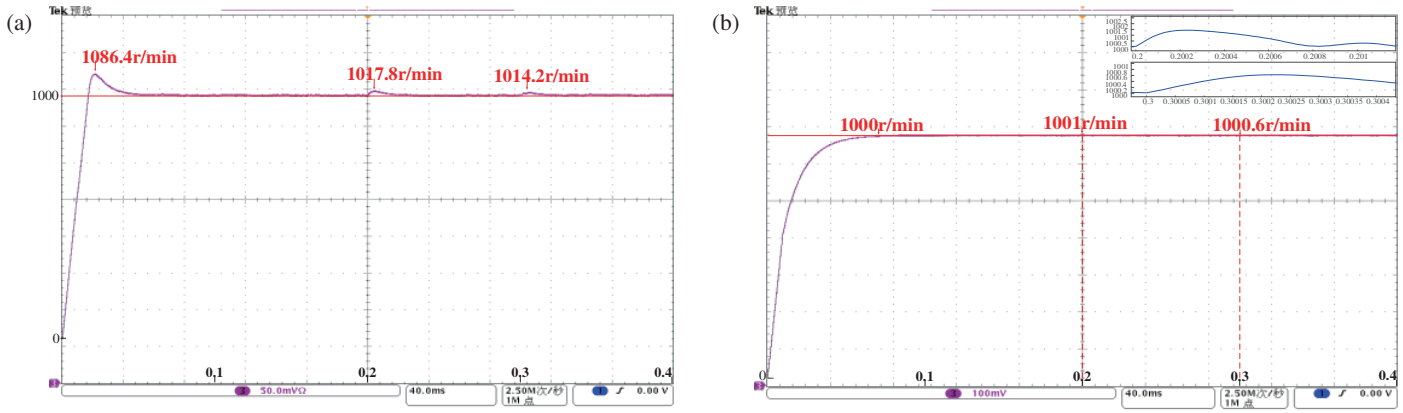


**FIGURE 5**. D-PMSG speed control experiment results. (a) Speed waveform with PI controller. (b) Speed waveform with LADRC controller.

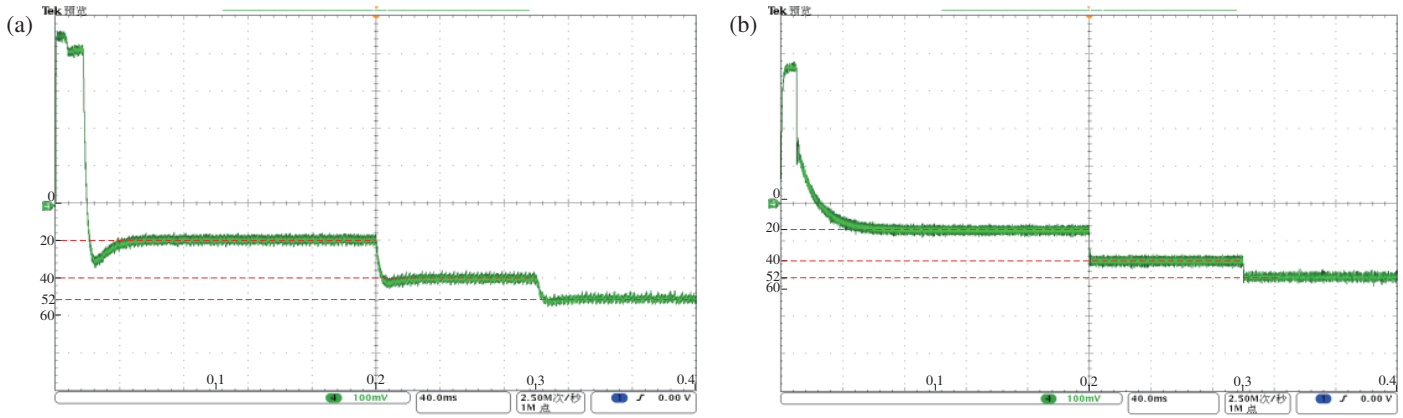


**FIGURE 6**. Experimental results of $q$-axis current of D-PMSG. (a) The $q$-axis current with PI controller. (b) The $q$-axis current with LADRC controller.

where $z_3$ and $z_5$ are used to estimate the values of $i_q$ and $i_d$, respectively; $e_3$ and $e_4$ are the errors between the estimated and actual values of the current; $z_4$ and $z_6$ are real-time estimates of the total perturbations $f_q$ and $f_d$, respectively, $f_d = 1/L_d\,[u_d - Ri_d + \omega_e(L_q i_q + \psi_{rq})] - b_d u_d$; $\beta_3$, $\beta_4$, $\beta_5$, $\beta_6$ are the output error correction gains; $k_{p2}$ and $k_{p3}$ are the control parameter; $u_{02}$ and $u_{03}$ are equivalent control volumes; $u_2$ and $u_3$ are the outputs of the LSEF link.

## 4. COMPARATIVE ANALYSIS OF EXPERIMENTAL RESULTS

In this paper, the suggested fault tolerance control strategy for demagnetization is empirically evaluated on an RT-LAB semi-physical control platform, which is based on RT-LAB, for comparison with conventional methods. DSPT320F2812 is employed as the controller, and the experiments on the Permanent Magnet Synchronous Generator (PMSG) are conducted using RT-LAB (OP5600). Experimental investigations encompassed both the conventional D-PMSG machine-side double closed-loop PI control and demagnetization fault-tolerant control strategies. Figure 4 provides a visual representation of the experimental platform used.

The parameters are presented in Table 1. The provided trial conditions are as described: the initial provided speed is $\omega* = 1000$ r/min; the initial provided mechanical torque is $T_L = 6$ N·m; the initial given magnetic chain $\psi_{r0} = 0.0485$. At 0.2 s, the mechanical torque increases to $T_L = 12$ N·m; at 0.3 s, demagnetization occurs; $\psi_r$ becomes 0.0385; the angle of deviation is converted to $\pi/6$.

**TABLE 1**. D-PMSG parameters.

| Parameters | Value |
|---|---|
| Stator inductance (mH) | 0.235 |
| Rated power (kW) | 2 |
| Rated line voltage (V) | 200 |
| Stator resistance (Ω) | 0.045 |
| Rotor inertia (kg·m$^2$) | 0.005 |
| Rated speed (r/min) | 1000 |
| Number of pole pairs | 4 |
| Stator current limit value (A) | 90 |

The simulation results of the rotational speed loop are shown in Figure 5. Figure 5(a) shows the speed waveform of D-PMSG under PI controller. The speed fluctuation is 86.4 r/min at startup, and the time from the start of the rise to return to a steady state is 0.06 s. The speed fluctuation is 17.8 r/min when the torque suddenly becomes larger. The demagnetization of permanent magnets results in the decrease of electromagnetic

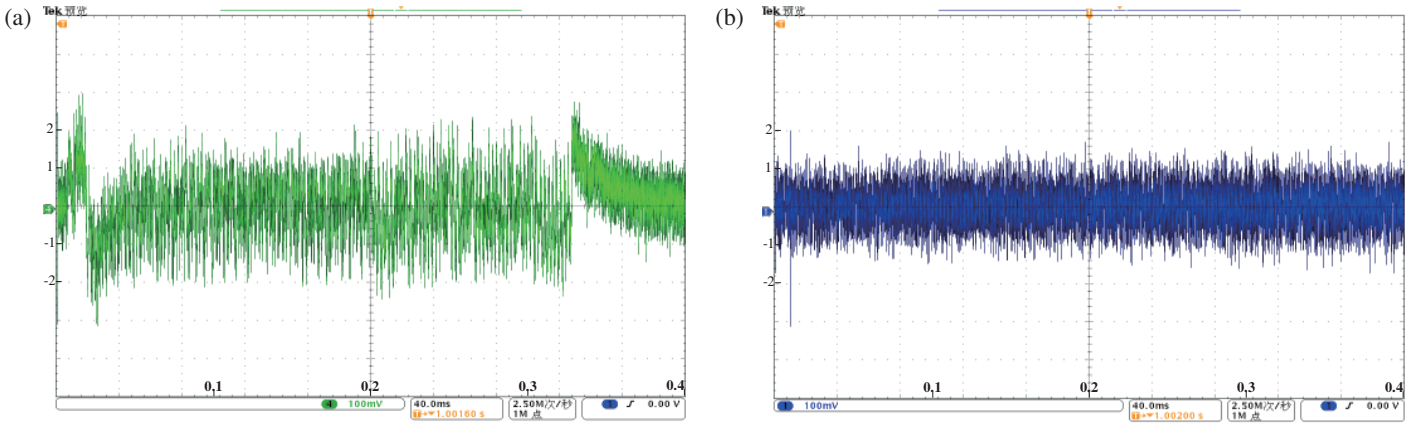


**FIGURE 7**. Experimental results of $d$-axis current of D-PMSG. (a) $d$-axis current with PI controller. (b) $d$-axis current with LADRC controller.

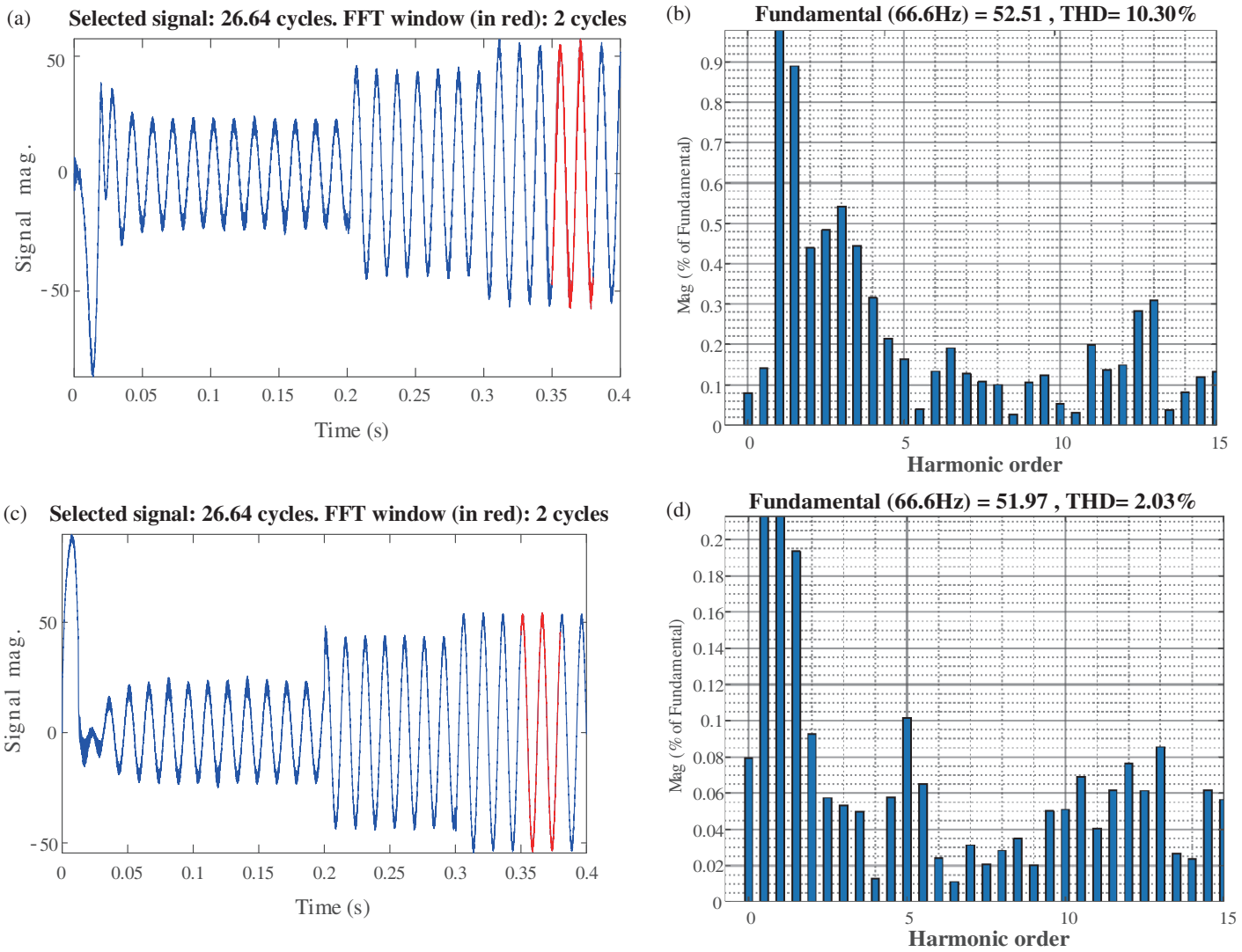


**FIGURE 8**. The diagram depicting A-phase current and harmonic analysis. (a) Generator phase currents with Fourier analysis under PI controller. (b) Generator phase currents with Fourier analysis under LADRC controller.

torque, leading to a speed fluctuation of 14.2 r/min. The entire speed adjustment process is about 0.05 s. Figure 5(b) shows the generator speed waveform under the LADRC controller. The speed is smooth throughout the process, and the speed fluctuation is only 0.6 r/min when demagnetization occurs with the duration less than 0.01 s. The strategy proposed in the paper

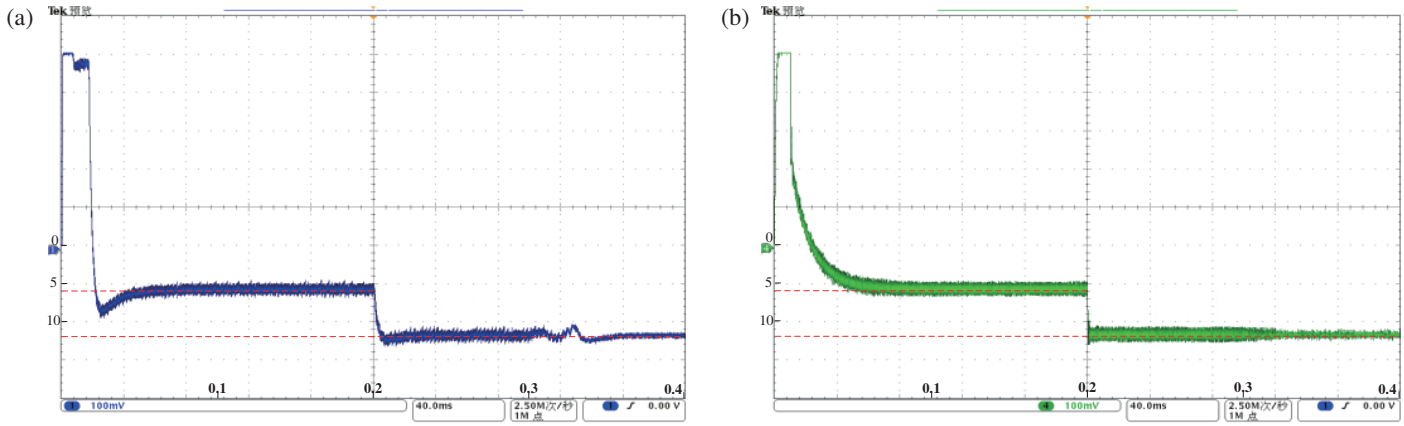


**FIGURE 9**. Experimental results of D-PMSG torque (a) Electromagnetic torque under double closed-loop PI control. (b) Electromagnetic torque under cascaded LADRC control.

**TABLE 2**. Comparison of experimental results between dual-closed-loop Proportional Integral (PI) control and cascaded linear active disturbance rejection control.

| | dual-closed-loop Proportional Integral (PI) control | cascaded linear active disturbance rejection control |
|---|---|---|
| speed fluctuation | 14.2r/min | 0.6r/min |
| the current response time | 0.01s | $<$0.001s |
| THD | 10.3% | 2.03% |
| the electromagnetic torque ripple amplitude | 8.3% | 4.1% |

basically eliminates the rotational speed fluctuation of the transient demagnetization process.

When demagnetization occurs, the generator compensates for the lost torque by increasing the $q$-axis current. The motor convention is used in the experiment. To facilitate comparative analysis, the current direction during steady-state operation is taken as the positive direction in the $q$-axis current experiment. We primarily compare the dynamic response time of the current after demagnetization. The current response time is 0.01 s with the PI controller and less than 0.001s with the LADRC controller. As shown in Figure 6(b), the current almost instantly reaches the compensation value under the LADRC controller. The $d$-axis current is controlled by $id = 0$. Figure 7 shows that the $d$-axis current under the PI controller exhibits significant oscillation, while the $d$-axis current under the proposed control method is smoother. The dynamic response speed and immunity of the current under the cascade LADRC strategy are higher than that of the conventional PI control method.

The A-phase current and harmonic analysis of the demagnetization fault-tolerant control strategy are illustrated in Figure 8. The waveforms and amplitudes of the currents after demagnetization in the two control modes are not significantly different. However, the current harmonic distortion (THD) under the LADRC controller is 2.03%, which is significantly lower than the THD under the double-loop PI control.

As shown in Figure 9, when torque pulsations after demagnetization are compared between the two control modes, it is observed that the maximum torque pulsation is approximately 8.3% under the PI controller, whereas it is only 4.1% under the LADRC controller. This comparative result indicates that the motor's immunity to interference is enhanced through the application of the cascaded LADRC strategy.

Table 2 summarizes the results of the experimental comparison between the dual-closed-loop Proportional Integral (PI) control and cascaded linear active disturbance rejection control. These experimental results fully validate the heightened fault tolerance and resistance to interference exhibited by the method advocated in this paper.

## 5. CONCLUSION

Aiming at the problems of poor dynamic performance, weak immunity, and speed fluctuations when the demagnetization occurs in the D-PMSG, a cascade LADRC control strategy was proposed. By experimentally comparing the cascaded LADRC control with the conventional dual closed-loop PI control of the D-PMSG wind turbine, the experimental conclusions obtained are as follows:

(1) Comparing the performance of cascaded LADRC control and dual-loop PI control on current. The LADRC controller enables fast tracking of the signal. $q$-axis current compensation for motors under LADRC control is faster when demagnetization occurs. $q$-axis current fluctuations are small, and the harmonic content of the demagnetized current is reduced. This controller is proved to have excellent control characteristics. Motor's immunity to interference and response speed are improved.

(2) Comparing the performance of cascaded LADRC control and dual-loop PI control on the rotational speed. The rotational speed under the LADRC can realize no overshooting in the dynamic process. Motor speed can be maintained smoothly when demagnetization occurs. The control method proposed in the paper solves the problem of speed fluctuation caused by generator demagnetization perturbation under conventional control. The torque pulsation after demagnetization is smaller. The fault-tolerant ability of the motor is stronger under this control strategy.

## ACKNOWLEDGEMENT

This work was supported by the Natural Science Foundation of Hunan Province of China under Grant Number 2023JJ50191, Educational Commission of Hunan Province of China under Grant Number 21B0552.

## REFERENCES

[1] Prince, M. K. K., M. T. Arif, A. Gargoom, A. M. T. Oo, and M. E. Haque, "Modeling, parameter measurement, and control of PMSG-based grid-connected wind energy conversion system," *Journal of Modern Power Systems and Clean Energy*, Vol. 9, No. 5, 1054–1065, September 2021.

[2] Osman, A. M. and F. Alsokhiry, "Sliding mode control for grid integration of wind power system based on direct drive PMSG," *IEEE Access*, Vol. 10, 26567–26579, 2022.

[3] He, S. and M. Wang, "Grey prediction pi control of direct drive permanent magnet synchronous wind turbine," *2020 IEEE 4th Conference on Energy Internet and Energy System Integration (EI2)*, 2032–2035, 2020.

[4] Ullah, Z. and J. Hur, "A comprehensive review of winding short circuit fault and irreversible demagnetization fault detection in PM type machines," *Energies*, Vol. 11, 3309, 2018.

[5] Meiwei, Z., L. Weili, and T. Haoyue, "Demagnetization fault diagnosis of the permanent magnet motor for electric vehicles based on temperature characteristic quantity," *IEEE Transactions on Transportation Electrification*, Vol. 9, No. 1, 759–770, March 2023.

[6] Barmpatza, A. C. and J. C. Kappatou, "Study of a combined demagnetization and eccentricity fault in an AFPM synchronous generator," *Energies*, Vol. 13, 5609, 2020.

[7] Zhou, P., D. Lin, Y. Xiao, N. Lambert, and M. A. Rahman, "Temperature-dependent demagnetization model of permanent magnets for finite element analysis," *IEEE Transactions on Magnetics*, Vol. 48, No. 2, 1031–1034, Feb. 2012.

[8] Ancuti, M.-C., S. Musuroi, C. Sorandaru, M. Dordescu, and G. M. Erdodi, "Wind turbines optimal operation at time variable wind speeds," *Applied Sciences*, Vol. 10, No. 12, 4232, 2020.

[9] Qi, L., L. Zheng, X. Bai, Q. Chen, J. Chen, and Y. Chen, "Nonlinear maximum power point tracking control method for wind turbines considering dynamics," *Applied Sciences*, Vol. 10, 811, 2020.

[10] Liu, H., "Wind power system for grid-connection based on PMSG and PI controlling under variable wind speed," *Journal of Physics: Conference Series*, Vol, 2254, No. 1, IOP Publishing, 2022.

[11] Imad, A., S. El Hani, A. Echchaachouai, and A. A. Energy, "Robust active disturbance rejection control of a direct driven PMSG wind turbine," *2017 International Renewable and Sustainable Energy Conference (IRSEC)*, 1–6, Tangier, Morocco, 2017.

[12] Bin, Z., *Introduction to Active Disturbance Rejection Control*, Beijing University of Aeronautics and Astronautics Press, 2017.

[13] Lin, P., Z. Wu, Z. Fei, and X.-M. Sun, "A generalized PID interpretation for high-order LADRC and cascade LADRC for servo systems," *IEEE Transactions on Industrial Electronics*, Vol. 69, No. 5, 5207–5214, May 2022.

[14] Ayadi, M., O. Naifar, and N. Derbel, "High-order sliding mode control for variable speed PMSG-wind turbine-based disturbance observer," *International Journal of Modelling, Identification and Control*, Vol. 32, No. 1, 85–92, 2019.

[15] Luo, B., S. Peng, Y. Zhang, et al., "A fault-tolerant control strategy for D-PMSG wind power generation system," *Progress In Electromagnetics Research C*, Vol. 123, 75–89, 2022.

[16] Li, S., J. Li, Y. Tang, et al., "Model-based model predictive control for a direct-driven permanent magnet synchronous generator with internal and external disturbances," *Transactions of the Institute of Measurement and Control*, Vol. 42, No. 3, 586–597, 2020.

[17] Han, J., "From PID technology to 'auto-disturbance control' technology," *Control Engineering of China*, Vol. 9, No. 3, 13–18, 2002.

[18] Gao, Z., "Scaling and bandwidth-parameterization based controller tuning," *ACC*, 2003.

[19] Zhou, K., M. Ai, Y. Sun, et al., "PMSM vector control strategy based on active disturbance rejection controller," *Energies*, Vol. 12, No. 20, 3827, 2019.

[20] Ma, R., X. Guo, Y. Zhang, and J. Gui, "PMSG offshore wind power system control using SMC and ADRC with fast SVPWM in complicated environment," *Electrical Engineering*, Vol. 105, 2751–2767, 2023.

[21] Lanhong, Z., Sheng, L., and Z. Qingjie, "Design of active disturbance rejection controller in speed loop for permanent magnet synchronous wind power generation system," *Control Engineering of China*, Vol. 29, No. 9, 1645–1651, 2022.

[22] Liu, C., G. Luo, Z. Chen, et al., "Measurement delay compensated LADRC based current controller design for PMSM drives with a simple parameter tuning method," *ISA transactions*, Vol. 101, 482–492, 2020.